NJC

Accepted Manuscript

This is an *Accepted Manuscript*, which has been through the Royal Society of Chemistry peer review process and has been accepted for publication.

Accepted Manuscripts are published online shortly after acceptance, before technical editing, formatting and proof reading. Using this free service, authors can make their results available to the community, in citable form, before we publish the edited article. We will replace this *Accepted Manuscript* with the edited and formatted *Advance Article* as soon as it is available.

You can find more information about *Accepted Manuscripts* in the Information for Authors.

Please note that technical editing may introduce minor changes to the text and/or graphics, which may alter content. The journal's standard Terms & Conditions and the Ethical guidelines still apply. In no event shall the Royal Society of Chemistry be held responsible for any errors or omissions in this *Accepted Manuscript* or any consequences arising from the use of any information it contains.

ROYAL SOCIETY OF CHEMISTRY

www.rsc.org/njc

Design of Dual Stimuli Responsive Polymer Modified Magnetic Nanoparticles for Targeted Anti-Cancer Drug Delivery and Enhanced MR Imaging

Dipsikha Bhattacharya[*a,c], Birendra Behera[b], Sumanta Kumar Sahu[d], Rajakumar Ananthakrishnan[a], Tapas Kumar Maiti[b] and Panchanan Pramanik[*,a]

1. Department of Chemistry, Indian Institute of Technology Kharagpur[a], West Bengal, India.
2. Department of Biotechnology, Indian Institute of Technology Kharagpur[b], West Bengal, India.
3. Nanotherapeutics Laboratory, CSIR-Indian Institute of Toxicology Research[c], Lucknow, India.
4. Department of Applied Chemistry, Indian School of Mines, Dhanbad, India[d].

* Corresponding author. E-mail: dipsikha.chem@gmail.com, pramanik1946@gmail.com; Phone no: +91-522-2620107, Fax no: +91-522-2628227

ABSTRACT

Herein, we report a strategic design of dual temperature and pH responsive polymer integrated magnetic nanohybrids comprising of smart block copolymer and mixed ferrite nanoparticles (MFNPs) for efficient anti-cancer drug delivery and magnetic resonance imaging (MRI). Citrate stabilized mixed ferrite nanoparticles (CA-MFNPs) were intelligently modified with the dual responsive Polyethyleneimine (PEI) cross-linked Pluronic F127 copolymer via EDC/NHS method. In order to accomplish cancer targeting and imaging capability, both the folic acid (FA) and rhodamine isothiocyanate (RITC) were tethered to the

nanoparticles *via* intricate chemical approaches. These FA targeted nanohybrids were further entrapped with doxorubicin (DOX) and investigated their release pattern. These DOX loaded FA targeted nanoparticles (DOX-FA-Poly-MFNPs) demonstrated high drug payload and encapsulation efficiency i.e. 4.6% and 92.0%, respectively. It is shown that at the lower pH/ higher temperature i.e. acidic pH (5.0) and at body temperature (37°C), the DOX-FA-Poly-MFNPs exhibited enhanced release of DOX (drug release value ~ 53%) while retaining their stealthy structure at physiological conditions, (drug release value ~ 12%) exhibiting an apparent thermo/pH controlled drug release pattern. The folic acid receptor (FAR) specific endocytosis to cancer cells (human cervix adenocarcinoma i.e. HeLa) in comparison to normal immortalized keratinocytes (HaCaT) cells were demonstrated via fluorescence microscopy and magnetic resonance imaging (MRI). Furthermore, these DOX-FA-Poly-MFNPs displayed effective therapeutic activity evaluated by cytotoxicity assay and cell cycle analysis in HeLa cells. Therefore, this dual responsive mixed ferrite nanoparticles may serve as a promising theranostic agent for *in-vivo* cancer therapy.

KEYWORDS: Mixed ferrite nanoparticles, Smart block copolymers, Doxorubicin, Drug delivery, Magnetic resonance imaging.

1. INTRODUCTION

Since the last decade, cancer research has envisioned that malignant cells exhibit an enhanced temperature and acidic microenvironment due to their rapid growth, providing a handle for pathological cells treatment with controlled drug release property. This concept has stimulated researchers towards the development of thermo, pH and dual stimuli-responsive polymeric nanomaterials (micelles, vesicles, gels) for cancer treatment [1-2]. Among

them, dual pH and thermo responsive nanocarriers have been striving forward as next generation therapeutic nanomedicines because they can intelligently trigger their release in stimuli responsive manner with minimal toxicity, improved therapeutic efficacy and reduced dosage to healthy cells [3-6]. Inorganic nanoparticles such as silica[7,8] and magnetic nanoparticles (MNPs) in forms of iron oxide as well as metal doped mixed ferrite nanoparticles integrated with dual responsive polymeric functionalities have gained emerging attention for a myriad of biomedical applications in simultaneous diagnosis and therapy [9-15]. Of late, there is a stride of developing intelligent theranostic systems using stimuli responsive polymers as delivery carriers and MNPs as MR imaging agents which can offer an improved target-guided delivery of therapeutics with synergistic package of specific targeting [15], MR based diagnostic imaging [16] and stimuli triggered delivery efficacy [17-18].

In the past decade, pH-responsive polymer embedded MNP nanocarriers have attracted profound attention as therapeutic carriers since there is a significant discrepancy in pH values in normal tissues (7.4)[19] and the acidic environment of both the extracellular (pH~6.8) and endosomal environments (~5.0−5.5) of tumor cells [20-21]. Additionally, temperature-responsive MNP nanocarriers[21] (exhibiting lower critical solution temperature ~ LCST) have also been widely studied because of their inherent capability to generate heat in the presence of applied magnetic field (AMF) [22] which can trigger the release of drugs from the polymeric carrier in tumor cells. To date, very limited reports are available on dual-responsive polymer modified MNPs harnessing both the pH [23-24] and thermo responsive [25-31] eminences of the synthesized polymer to MNPs [29-32]. In addition; it is also noteworthy that in most of the cases, poly (N-isopropylacrylamide) (PNIPAAm) or poly (N-vinylcaprolactam) (PVCL) has been used as thermo sensitive polymers [29-32]. Recently, our lab has also reported a dual

responsive MNPs as drug delivery carrier utilizing PNIPAAm as the surface activating polymer[31]. Of late, Patra et al. also reported a dual responsive polymer (poly N-isopropylacrylamide-co poly glutamic acid) coated mixed ferrite nanosystems for drug delivery applications[33].

Among the block copolymers, triblock copolymer Pluronic, consisting of both hydrophobic poly (propylene oxide) (PPO) and hydrophilic poly (ethylene oxide) (PEO) blocks, have been widely acclaimed as thermo responsive delivery nanocarriers for both *in vivo* and *in vitro* drug delivery applications [32,34-38]. Similarly, Polyethylene imine (PEI), a highly acclaimed pH responsive polymer [39], has already been used in various modifications for drug/gene delivery applications [38-40]. Recently, Liu et al. has reported Pluronic crosslinked PEI (PF127-PEI) block copolymer stabilized magnetic nanosystems as a thermoresponsive drug delivery carrier[27], however, as par our knowledge concerned, no one has embarked on the development of PF127-PEI tethered MNPs as dual delivery systems.

In addition, along with the concern of delivery of therapeutics, development of enhanced MR based diagnostic imaging for cancer monitoring is also of prime concern to visualize, tract and monitor the disease at its earliest stages. MNPs especially Mn doped mixed ferrite nanoparticles (MFNPs) have drawn attention as ultrasensitive T_2 contrast agents to enhance the sensitivity of non-invasive MRI imaging[41]. On the light of this advantage, we envisioned that this PEI-PF127 polymer tethered MFNPs as a theranostic nanocarriers would be of great interest, due to its potential advantage in delivering therapeutics in a intelligent manner distinguishing normal and pathological cells, triggered release of cargos in a stimuli responsive manner along with enhanced monitoring efficacy.

To achieve the target, a strategic design for the fabrication of dual responsive mixed ferrite nanohybrids is proposed and followed by further integration/encapsulation with targeting agent (FA), fluorescence imaging dye i.e. rhodamine B isothiocyante (RITC) and doxorubicin (DOX) as the anticancer drug. In particular, dual responsive polymer i.e. PEI-PF127 was synthesized using simple conjugation approach and latter tethered to citrate stabilized mixed ferrite MFNPs (CA-MFNPs). Thereafter, FA and RITC was conjugated to aminated PEI-PF127-MFNPs (Poly-MFNPs) to endow the carrier with cancer targeting and optical imaging ability. Finally, therapeutic agent, DOX molecules has been encapsulated inside the hydrophobic cores of the nanocarriers to construct the targeted nanomedicine. Since most tumor sites usually exhibit a more acidic environment or a higher temperature, the dual pH and thermo-responsive releasing efficacy of the DOX entrapped nanoparticles can be triggered enhanced drug release at a tumor region than a normal one. The resulting nanocomposites have several advantages such as high drug entrapment efficiency, enhanced FAR targeting and stimuli triggered cargo release ability to acidic cancer cells along with the MR assisted intracellular tracking ability. As far our knowledge concerned, this is the first attempt of a dual responsive polymer modified targeted nanomedicine (DOX-FA-Poly-MFNPs) with cancer targeting, stimuli responsive drug delivery and enhanced MR imaging ability.

2. RESULTS AND DISCUSSIONS

2.1 Synthesis and Characterization of dual responsive theranostic mixed ferrite nanoparticles:

The goal of this work was to design and develop a dual pH and temperature responsive polymer modified targeted nanomedicine (DOX-FA-Poly-MFNPs) for the targeted delivery of the anticancer drug doxorubicin (DOX) in a stimuli triggered fashion and to achieve

enhanced MR imaging. The step wise illustration involved in the fabrication of this magnetic nanomedicine has been shown in Scheme 1.

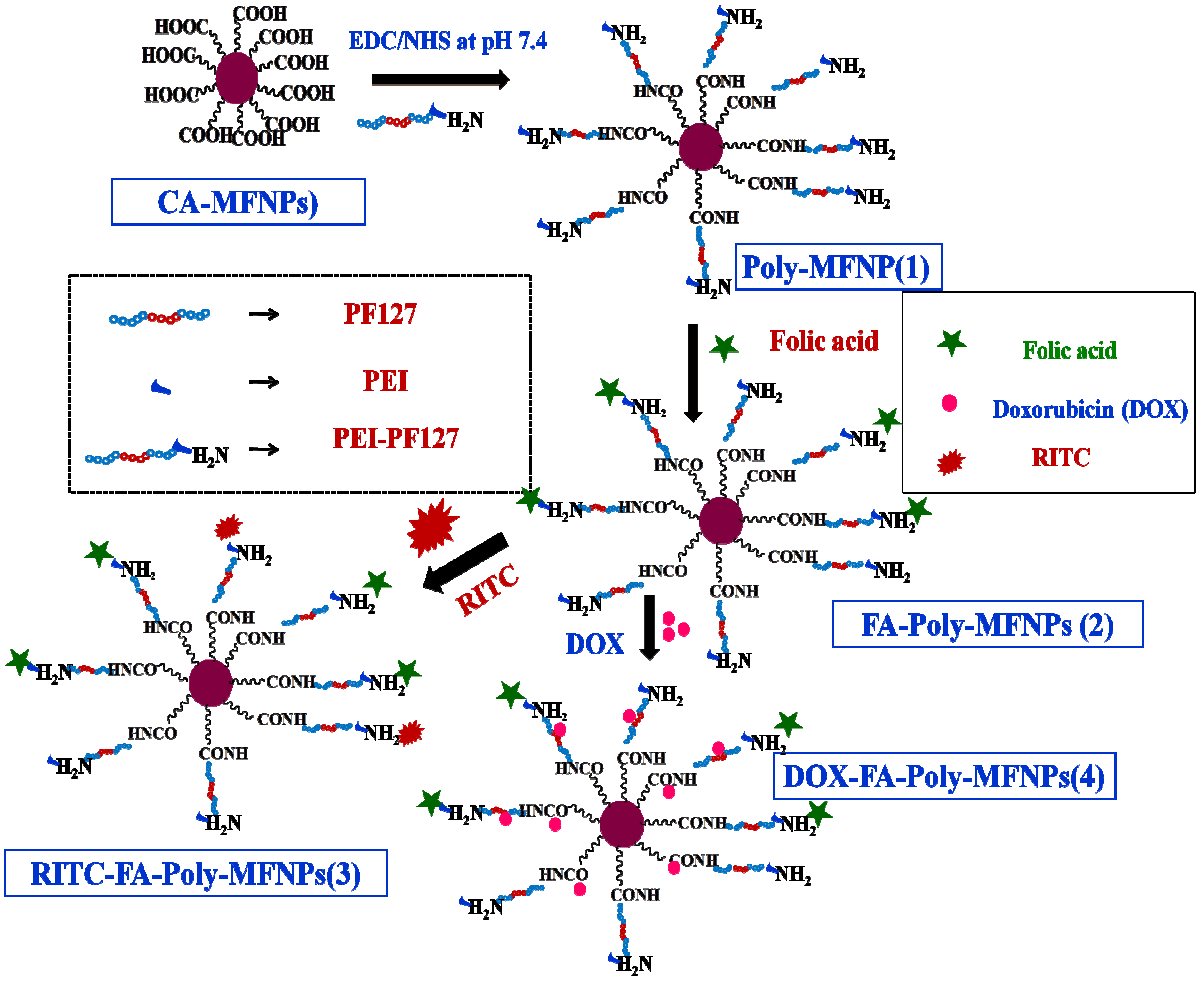

Scheme 1: Schematic illustration of fabrication of dual pH and temperature responsive Poly-MFNPs and their subsequent conjugation with folic acid, RITC and DOX to fabricate a multifunctional nanomedicine.

To fabricate dual responsive mixed ferrite particles described as PEI-PF127-MFNPs or Poly-MFNPs (**1**), monodispersed mixed ferrite nanoparticles (MFNPs) were synthesized by aqueous co-precipitation approach in presence of trisodium citrate. For the synthesis of dual responsive copolymer, Pluronic F127 (PF127) has been chosen as the thermo responsive

polymer because of its lower LCST facilitating the self assembly formation around body temperature due to the temperature responsive hydration/dehydration phenomena[27]. Polyethyleneimine (PEI) was chosen because of its manifold role of pH responsive nature due to its well known proton sponge effect and also its functional amine donating efficacy [42]. Amine functionalities of the dual responsive PEI-PF127 copolymer were covalently tethered to the citrate stabilized mixed ferrite MFNPs (CA-MFNPs) using EDC/NHS chemistry[43]. Furthermore, the cancer targeting property was introduced in these Poly-MFNPs through folic acid (FA) tethering via EDC/NHS approach[44]. Both of the FA targeted (FA-Poly-MFNPs) and non targeted (Poly-MFNPs) were also labelled with RITC by covalent linking[45] utilizing some of the residual surface amine groups imparting RITC-Poly-MFNPs and RITC-FA-Poly-MFNPs respectively.

The high resolution X-ray diffraction pattern of CA-MFNPs (Figure S1 in Electronic Supporting Information i.e. ESI) depicted the broadening of peaks with small crystalline sizes of the nanoparticles, (an average core size of about 4-6 nm) using the Debye–Scherrer formula for spherical particles. The size distribution and morphology of these Poly-MFNPs (**1**) were examined by transmission electron microscopy (TEM) analysis. Fig. 1(A-B) displayed the TEM images of CA-MFNPs and Poly-MFNPs (**1**). Fig. 1(A) demonstrated that before polymeric modification, the size of the CA-MFNPs were in between 8±2 nm whereas after modification, these Poly-MFNPs showed a size enhancement as well as presence of a thin polymer layer depicting their successful modification (~12 nm) [Fig. 1(B)].

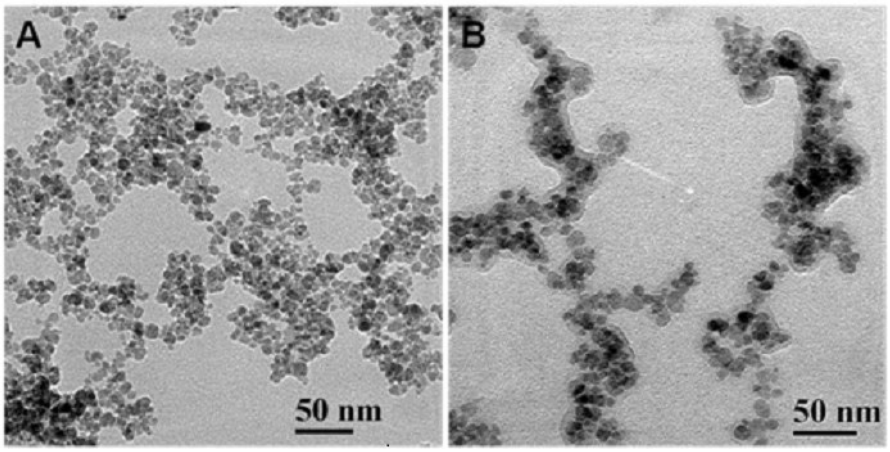

Fig. 1: A) and B) TEM images of CA-MFNPs and Poly-MFNPs.

However, some agglomeration appeared in case of Poly-MFNPs due to their high magnetization and surface energy, although was comparatively lower respect to CA-MFNPs. The uniform hydrodynamic sizes (HDs) and surface charges of these Poly-MFNPs (**1**) at physiological pH were observed around 80±10 nm (PDI ~ 0.213) and 14.5mV reflecting good stabilization of these Poly-MFNPs. After FA modification, the moderate increase in HD of FA-Poly-MFNPs (**2**) (~91 nm) and decrease in positive charge (-12.5mV at pH 7.4) demonstrated these FA-Poly-MFNPs were functionalized with carboxylate groups that endowed enhanced hydrogen bonding efficacy compared to **1** nanoparticles. [The detailed description of DLS and zeta potential of these nanoconjugates was included in the ESI in Table S1 and Figure S2 (A)].

The pH responsive nature of our nanoconjugates (Poly-MFNPs and FA-Poly-MFNPs) was validated by measuring their effective hydrodynamic diameters (HDs) and surface charge analysis under various pHs at room temperature (RT). (See Figure S2 (A) i.e. Zeta potential vs. pH and (B) i.e. HD change vs. pH in the ESI). It was observed that the surface charges and HDs of Poly-MFNPs showed an enhancement from 14.5mV

to 35.5 mV and 81 nm to 113 nm when pH was decreased from 7.4 to 5. These phenomena might be due to the extensive protonation of the PEI residues of Poly-MFNPs due to its proton sponge effect, which resulted in an electrostatic repulsion between the immobilized -NH_2 groups of the polymer. Thus, these Poly-MFNPs inevitably underwent swelling under acidic pH ~ 5, which can eventually accelerate the disruption of cargos entrapped in the nanohybrids[38]. Therefore, the results showed that these Poly-MFNPs could endow pH responsive property. In order to check whether the pH responsive nature retained or not, these FA-Poly-MFNPs (**2**) were also thoroughly checked with changes in HD vs. pHs and also zeta potential vs. pHs. It was shown in [Figure S2 (A) and (B)] that at pH ~ 5, these **2** exhibit reasonable HD changes (105 nm) and high positive charge (+22.5 mV) as compared to their value from physiological pH (91.5nm and -12.5 mV). It was assumed that at lower pH, presence of both functional $–NH_3^+$ and $–CO_2H$ groups on FA-Poly-MFNPs counter balanced the drastic HD change as compared to Poly-MFNPs (113 nm at pH 5), although displayed the same pH responsive nature. Contrastingly, with increasing pH, most of their carboxylate groups of **2** exhibit repulsion between the functional $–CO_2H$ groups, reflected by their enhanced change in HD and surface charge (103 nm and -19.6 mV at pH 9). This HD change at higher pH was reasonably larger compared to Poly-MFNPs (91 nm). Therefore, it was clear that both of these nanoparticles showed almost similar response at lower pH values while at higher pH, the FA-Poly-MFNPs exhibited considerable discrepancy indicating the presence of $–CO_2H$ groups.

Likewise, the thermo responsive nature of our nanohybrids (both Poly-MFNPs and FA-Poly-MFNPs) was illustrated with the variation of HDs under different

temperatures at physiological pHs (See Figure S2 (C) in ESI). The volume average HDs of Poly-MFNPs underwent a sharp decrease from 85 to 31 nm with the increasing temperature 2°C to 45°C. This temperature responsive phenomenon might be attributed due to the thermally induced self assembly of the PF127 (PEO-PPO-PEO) segment of the copolymer and was harmonized well with the previously reported stimuli responsive Pluronic block copolymers [27,38]. At relatively low temperatures, the PF127 chains of Poly-MFNPs were fully extended via interacting with water molecules, facilitating the entrapment of drug molecules into the vector. While with increasing temperature above critical micelle concentration (CMC), a dehydration process of polymer blocks was induced resulting the effective clustering of PPO blocks [27, 46-47]. Thus, at the temperature close to the body temperature (37°C), the polymer shell of Poly-MFNPs got contracted, forming compact nanostructure, which would reflect in the decrease of the HDs with increasing temperature. As the thermoresponsive nature depends on the PF127, it was assumed that after FA modification, as the polymer PF127 segment remains intact, therefore the FA-Poly-MFNPs must exhibit the similar pattern of changes with respect to HD vs. Temperature.

The successful consecutive modifications of MFNPs using citric acid (CA-MFNPs), PEI-PF127 as well as FA, were evaluated by FTIR analysis. The FTIR spectra of CA-MFNP, PEI-PF127-MFNPs i.e. Poly-MFNPs (**1**), bare FA, and FA-PEI-PF127-MFNPs i.e. FA-Poly-MFNPs (**2**) were shown in Fig. 2. (The FT-IR spectra of activated PF127 and PEI-PF127 were given in Figure S3). For CA-MFNPs, the broad band, around 1630 cm^{-1} and a small

peak around 1715 cm^{-1} confirmed the successful modification of the mixed ferrite surface with carboxylate groups [48].

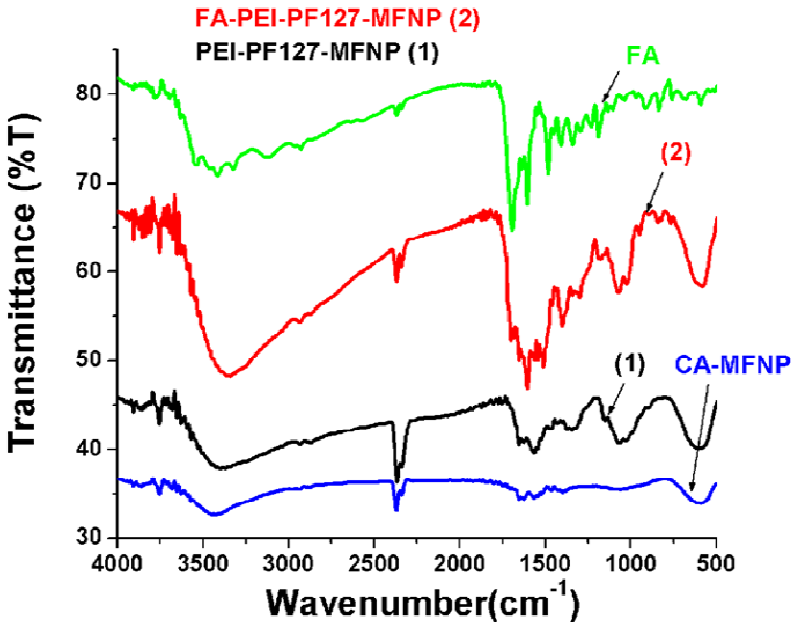

Fig. 2. FT-IR spectra of CA-MFNPs, PEI-PF127-MFNPs (Poly-MFNPs), FA-PEI-PF127-MFNPs (FA-Poly-MFNPs) and free Folic acid (FA).

A strong absorption band of M-O bonds was also observed at 590 cm^{-1} in this spectrum, indicating the successful formation of MFNPs. The spectrum of Poly-MFNPs (**1**) showed not only the main characteristic band of M-O but also the characteristic peaks of polymer at 1657 and 1563 cm^{-1} indicating the formation of the amide band. The bands at 1626 cm^{-1} and a broad band at 3400 cm^{-1} validated the presence of primary amine groups on **1** [45]. Hence, these results portrayed that the PEI-PF127 polymer was successfully immobilized onto the surface of CA-MFNPs. The FTIR spectrum of pure FA was characterized by a number of characteristic bands according to previously reported literature [49]. In the FTIR spectrum of FA-Poly-MFNPs (**2**), the peaks at 1654 cm^{-1} (bonded C=O of –CONH amide band II) and 1564 cm^{-1} (–NH amine band II) appeared with increased absorbance, generated from the

amide bands within the FA structure as well as the amide bonding between FA and amine-functionalized nanoparticles. Both the absence of a band at 1629 cm^{-1} and the presence of sharp bands at 1687, 1605 and 1401 cm^{-1} hereby confirmed the successful conjugation of FA to these Poly-MFNPs. Further, to demonstrate the modification of FA on Poly-MFNPs, the folate content on **1** and **2** were conveniently compared with a standard FA absorbance, attributing to folate only. (As shown in Figure S4). It is already known that Pure FA showed two peaks at 280 and 360 nm due to n−π* and π−π*transitions, respectively. [Given as Figure S4 (inset Figure) in ESI]. After modification with FA, these two peaks were observed with a little shift, signifying the successful modification with folic acid.

The formation of the as mentioned surface-modified nanoparticles was further corroborated by Thermal Gravimetric analysis (TGA) measurements. Step-wise weight loss from the nanoparticles with increasing temperature (Supporting Information, Figure S5) could be explained depending on the decomposition of the surface functionalities introduced at various stages. To authenticate the feasibility and sensitivity of Poly-MFNPs (**1**) as enhanced MR imaging nanoprobes, it is crucial that MFNPs should retain their favourable magnetic properties after surface modification. The magnetic properties of CA-MFNPs, Poly-MFNPs and FA-Poly-MFNPs have been evaluated using Vibration Sample Magnetometry (VSM) analysis (as depicted in Figure S6). The results corroborated that after modification with stimuli responsive polymer, Poly-MFNPs exhibited superparamagnetic nature with reduced magnetization compared to CA-MFNPs signifying their successful modification. Moreover, surface functionalization was performed further and confirmed by XPS studies. A detail explanation of XPS spectra and analysis is given in Supporting Information (Figure S7).

2.2. Fabrication of DOX loaded targeted nanomedicine (DOX-FA-Poly-MFNPs) and their dual responsive drug release phenomena:

Doxorubicin (DOX) was employed as a model drug to investigate the loading and release profile of the dual responsive Poly-MFNPs. The DOX loading was thoroughly standardized by varying DOX concentrations (0.2 mg/ml to 1 mg/ml) (Data not shown) with 10 mg FA-Poly-MFNPs and the best ratio of DOX:FA-Poly-MFNPs obtained was 20:1. The loading content and entrapment efficiency of DOX in FA-Poly-MFNPs were found to be 4.6% and 92.0%, respectively. It was previously reported that DOX can be loaded inside nanocarriers via both hydrophobic/ionic interactions [46] as well as covalent pH sensitive bonding[50-51]. In our case, entrapment of DOX in FA-Poly-MFNPs (**2**) was due to the combined hydrophobic and hydrogen bonding interactions between DOX molecules and PEI-PF127. In order to validate the dual responsive property of poly-MFNPs, *in vitro* DOX release from DOX-FA-Poly-MFNPs (**4**) was investigated at varied pHs i.e. physiological and lysosomal pH (pH 7.4 and 5.5) and varied temperatures (25 and 37°C) [Fig. 3(A)]. The stimuli triggered release mechanism of DOX from DOX-FA-Poly-MFNPs was well represented in Scheme 2.

For temperature controlled release, at pH 7.4, nearly, 11-12% DOX was released at 37ºC after 24 h whilst, 23% drug was released at 25°C from DOX-FA-Poly-MFNPs (**4**). On the contrary, at pH 5.5, about 31% of the loaded DOX was released after 24 h at 25°C, whereas, 53% was released at the same time interval at 37°C. From this, it was speculated that the cumulative drug release was enhanced at lysosomal i.e. acidic pH compared to physiological pH at body temperature. The block copolymer exhibited the combined and complementary role of a stimuli responsive drug delivery carrier where the PF127 segment was merely

responsible for the fabrication of thermoresponsive compact Poly-MFNPs at body temperature while PEI plays the pH responsive role. The slower DOX release at the

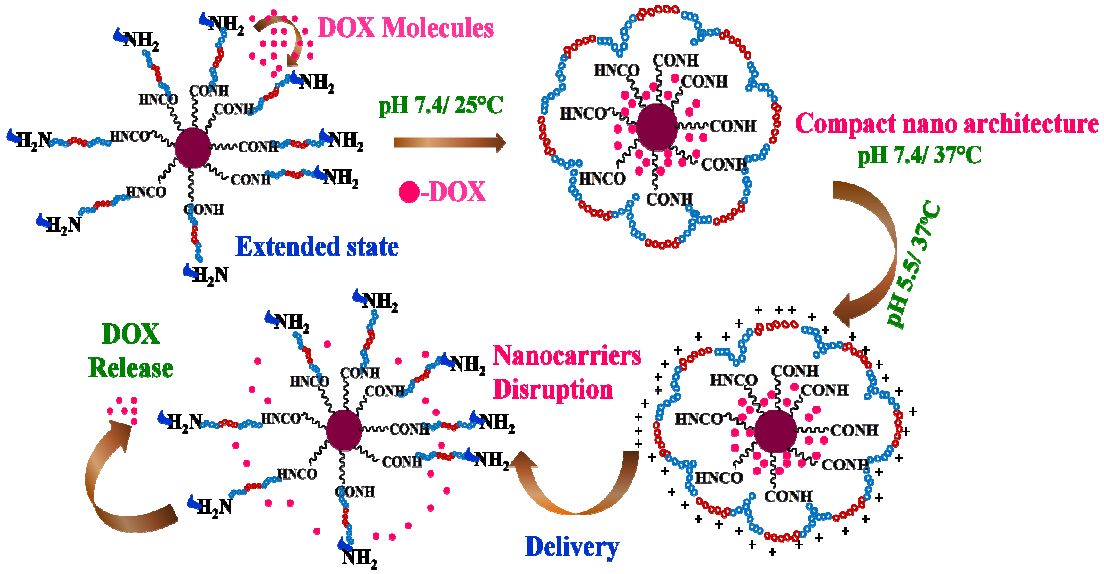

Scheme 2: Proposed presentation of dual temperature and pH responsive formation of self assembled Poly-MFNPs nanocarriers and the stimuli triggered release of doxorubicin through disruption of Poly-MFNPs at acidic pH and physiological temperature.

physiological temperature (37°C) and pH 7.4 authenticated the supreme stability of DOX-FA-Poly-MFNPs as an ideal delivery carrier. Due to the temperature responsive self assembly behaviour, at 25°C, the DOX molecules were entered inside the self assembled nanoparticles through the extended polymeric shell while with increasing temperature above the LCST, the shell was contracted, imparting the compact structure of DOX-FA-Poly-MFNPs, entrapping the loaded DOX molecules[27, 46]. When these compact DOX-FA-Poly-MFNPs were delivered to tumor cells, at the lysosomal pH ~5.5, the proton sponge effect of PEI exhibited protonation in the -NH_2 groups of PEI segments of DOX-FA-Poly-MFNPs, which resulted in enhanced electrostatic repulsion followed by swelling between the particles. This phenomenon subsequently triggered the release of drugs followed via the

disruption of DOX-FA-Poly-MFNPs and the DOX molecules would come out in a controlled fashion in cancer cells at body temperature [2, 38]. On the contrary, at pH 7.4, the almost neutrally charged DOX particles displayed negligible extent of release restraining the degradation of these DOX-FA-Poly-MFNPs (**4**) during blood circulation. Thus, at body temperature, the DOX-FA-Poly-MFNPs i.e. **4** nanoparticles were highly stable at pH 7.4 but were degraded when the pH was lowered to 5.5, mimicking lysosomal pH of acidic tumor cells. The drug release pattern reflected that the dual responsive polymer exhibited a key role on both the loading as well as release of loaded drug in a desired fashion.

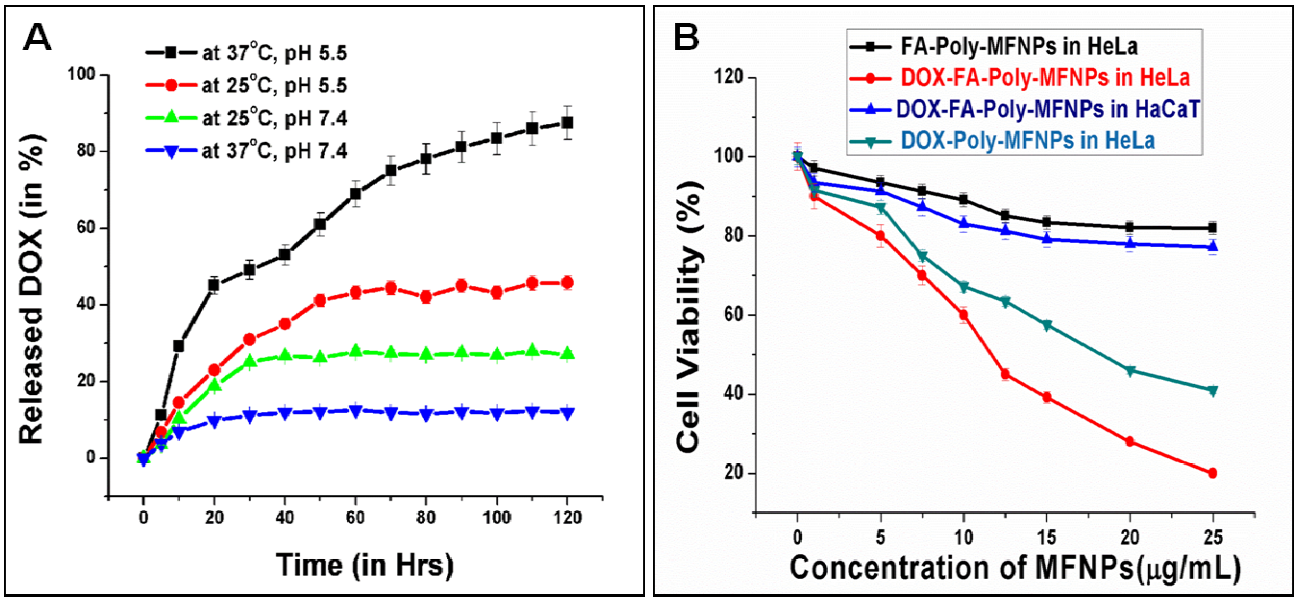

Fig. 3(A-B) A) Stimuli triggered release pattern of DOX from DOX-FA-Poly-MFNPs at different pH and temperature conditions. **(B)** Cell Cytotoxicity Assay of HeLa and HaCaT cells treated with FA-Poly-MFNPs, DOX-Poly-MFNPs and DOX-FA-Poly-MFNPs at different concentrations. Cell toxicity is measured by MTT assay at 570 nm.

2.3. Biological evaluation of targeted, non-targeted and DOX-loaded Nanoparticles.

2.3.1. Evaluation of therapeutic efficacy of DOX-FA-Poly-MFNPs.

Prior to evaluation of the anticancer activity of DOX-FA-Poly-MFNPs, cellular viability of Poly-MFNPs (**1)** and FA-Poly-MFNPs (**2)** have been evaluated in cancer HeLa-HFAR (High Folic acid Receptor) and normal HaCaT cells to prove that these nanocarriers are not cytotoxic (Figure S8, description given in ESI) and hence can be used for further *in vitro* and *in vivo* applications.

In contrast, the DOX-FA-Poly-MFNPs (**4**) and DOX-Poly-MFNPs showed significant cytotoxicity to cancer HeLa (HeLa-HFAR) cells after 24 h incubation. It was observed that the DOX-FA-Poly-MFNPs (**4**) induced almost 81% killing of HeLa cells [as shown in Fig. 3(B)]. DOX-Poly-MFNPs without FA also has caused more than 50% growth inhibition at 25μg/mL, although was comparatively lower than DOX-FA-Poly-MFNPs. whereas, at the same concentration (25μg/mL), the DOX-FA-Poly-MNPs (**4**) are almost cytocompatible in normal HaCaT cells. The half maximum inhibition concentration (IC_{50}) value of **4** is 12.5 μg/mL in HeLa cells.

Further to check whether the higher death in HeLa cells was due to the FA targeted receptor mediated endocytosis,[52] same concentration dependent study has been performed using synthesized DOX-FA-Poly-MFNPs and DOX-Poly-MFNPs without FA in HeLa-HFAR and HeLa cells expressing low Folic acid receptor (HeLa-LFAR) for 2h treatment (Shown in Fig. 4).

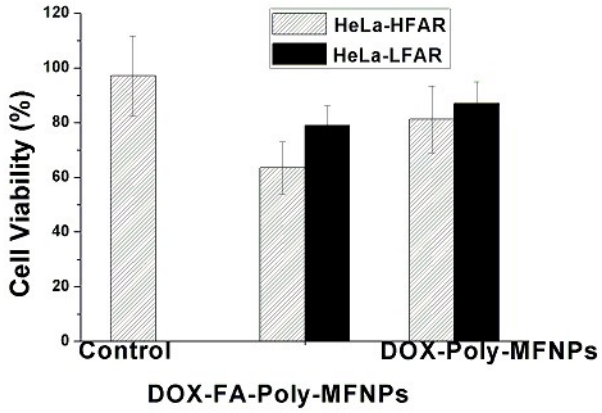

Fig. 4 Study of Folic acid receptor (FAR) targeting efficiency of DOX-FA-Poly-MFNPs and DOX-Poly-MFNPs into HeLa-HFAR (Highly FAR overexpressed) and HeLa-LFAR (Low FAR overexpressed) cells.

It was shown that after 2h incubation, the DOX-FA-Poly-MFNPs (25µg/ml) showed effective toxicity (around 63% viable) in HeLa-HFAR cells, while the DOX-Poly-MFNPs were significantly less toxic to HeLa-HFAR (81% viable cells) signifying that this higher toxicity of DOX-FA-Poly-MFNPs was mainly controlled due to FA modification because both were incubated with the same origin of HeLa cells. On the other hand, treated with either DOX-FA-Poly-MFNPs or DOX-Poly-MFNPs, in both the cases, HeLa-LFAR showed almost considerable amount of viable cells, indicating less targeting effect to HeLa-LFAR cells. Therefore, it could be authenticated that targeting efficiency of DOX-FA-Poly-MFNPs was due to FAR mediated internalization to HeLa cells over expressing high percentage of Folate receptors (HeLa-HFAR) and induced higher cell death.

2.3.2. Folate receptor mediated cellular internalization study.

The time dependent intracellular uptake of FA-Poly-MFNPs (**2)** and Poly-MFNPs (**1)** was analyzed by fluorescence microscopy. The target RITC-FA-Poly-MFNPs (**3**) and control

RITC-Poly-MFNPs (concentration 10μg/ml) were incubated in HeLa cells over expressing high FAR in folate free medium (HeLa cells over expressing HFAR) for 0h, 30 min, 1h, 2 h, and 4 h to evaluate the time-dependent cellular internalization of nanoparticles. Fig. 5(a-e) showed that with increasing incubation time, the red colored **3** were found to be distributed more intensifically near the nucleus of HeLa cells compared to the control RITC-Poly-MFNPs nanoparticles, suggesting enhanced cellular internalization in HeLa-HFAR cells. This study unambiguously established that the presence of FA on the fabricated **3** play the key role towards the folate receptor targeted internalization into HeLa cells compared to control nanoparticles i.e. RITC-Poly-MFNPs [45]. Further, to demonstrate the FAR targeting ability of RITC-FA-Poly-MFNPs in comparison to normal HaCaT cells, the cellular internalization was also cross verified using HeLa-HFAR and FAR negative HaCaT cells for 4h. [Detailed description and data were given as Figure 9(A-B) in ESI]. Though the FAR targeting ability was validated via performing cytotoxicity assay using DOX-FA-Poly-MFNPs and control DOX-Poly-MFNPs to HeLa-HFAR cells, in order to revalidate the ambiguous uptake in presence of free FA (i.e. HeLa-LFAR), the intracellular uptake of **3** in presence and in absence of FA (i.e. HeLa-HFAR) have been cross verified using fluorescence imaging analysis. [Detailed description and data were given as Figure 10(A-B) in ESI].

2.3.3. MR based Diagnostic imaging analysis.

To evaluate these FA-Poly-MFNPs as T_2 contrast MRI agents, *in vitro* MR imaging has been performed. The T_2-weighted phantom images of HeLa cells incubated with targeted FA-Poly-MFNPs (**2)** exhibited a significant negative contrast enhancement (signal darkening) in comparison to the MR image obtained for **2** treated HaCaT cells, suggesting its significant

internalization to folate receptor positive HeLa-HFAR cells. [As shown in Fig. 6(A)]. This distinguishable darkening of T_2 weighted MR images of the **2** in HeLa cells was rationalized due to folate receptor mediated endocytosis. The enhanced MR imaging efficacy of targeted **2** has also been verified with targeted magnetite nanoparticles (MNPs) synthesized without Mn doping. The MR images revealed that for the targeted FA-Poly-MFNPs (**2**), the signal darkening effect was higher compared to the similarly sized targeted FA-Poly-MNPs, though folate moiety was present in both the nanoconjugates. This may be attributed due to the higher magnetization value of the similarly sized MFNPs compared to MNPs only [51].

.

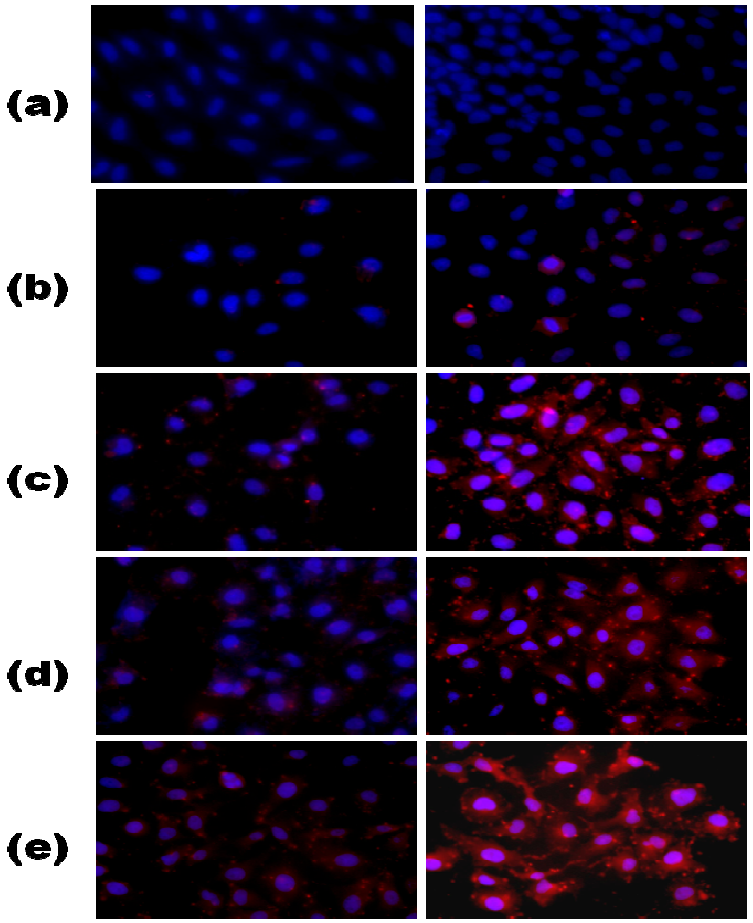

Fig. 5(a-e): Fluorescence images of uptake of HeLa-HFAR cells incubated with RITC-Poly-MFNPs and RITC-FA-Poly-MFNPs after (a) 0 min (b) 30 min (c) 1 h (d) 2 h e) 4h incubation.

The relative T_2 relaxation times of target FA-Poly-MFNPs (**2)** as well as control Poly-MFNPs (**1)** nanoparticles in HeLa-HFAR and HaCaT cells were also evaluated with increasing concentrations (0-30μg/ml). Fig. 6(B) showed the T_2-relaxation time as a function of particle concentration (**1** and **2**) in cell-culture media. HeLa cells cultured with target (**2**) nanoparticles possessed a shorter T_2-relaxation time compared to HaCaT cells, which was probably arising due to enhanced magnetism, germinated probably from the higher internalization of **2** by HeLa cells in comparison to the same in HaCaT cells. It was also observed that HeLa cells cultured targeted **2** had a shorter T_2 relaxation time than the targeted-Poly-MNPs due to enhanced magnetism of the similar sized Mn-doped mixed ferrites nanoparticle. It was further observed that the relaxation rate $1/T_2$ varied linearly with the iron concentration (equation no 2 given in experimental section). The transverse relaxivity, r_2 of the targeted **2** in HeLa cells (corresponding to the slope of the line) was found to be 184.22 $mM^{-1}s^{-1}$ respectively and it was found more than three times higher compared to FA-Poly-MNPs (60.12 $mM^{-1}s^{-1}$) in HeLa cells as shown in Figure S11(B). All these results unequivocally established the potential of our as-prepared FA-Poly-MFNPs as cancer-targeted, MRI probes.

2.3.4. FA targeted cancer cell inhibition via cell cycle analysis and apoptosis study

To further evaluate the antiproliferative action of DOX-FA-Poly-MFNPs (**4**) on HeLa-HFAR cells, cell cycle analysis and DNA fragmentation study i.e. apoptosis studies have been performed using propidium iodide (PI) and DAPI staining. From cell cycle analysis, early apoptosis and the phases of cell death could be investigated. For this,

HeLa cells were incubated with FA-Poly-MFNPs (at highest concentration ~ 25µg/mL, free DOX (10µg/mL) and DOX-FA-Poly-MFNPs (3.25 to 25 µg/mL).

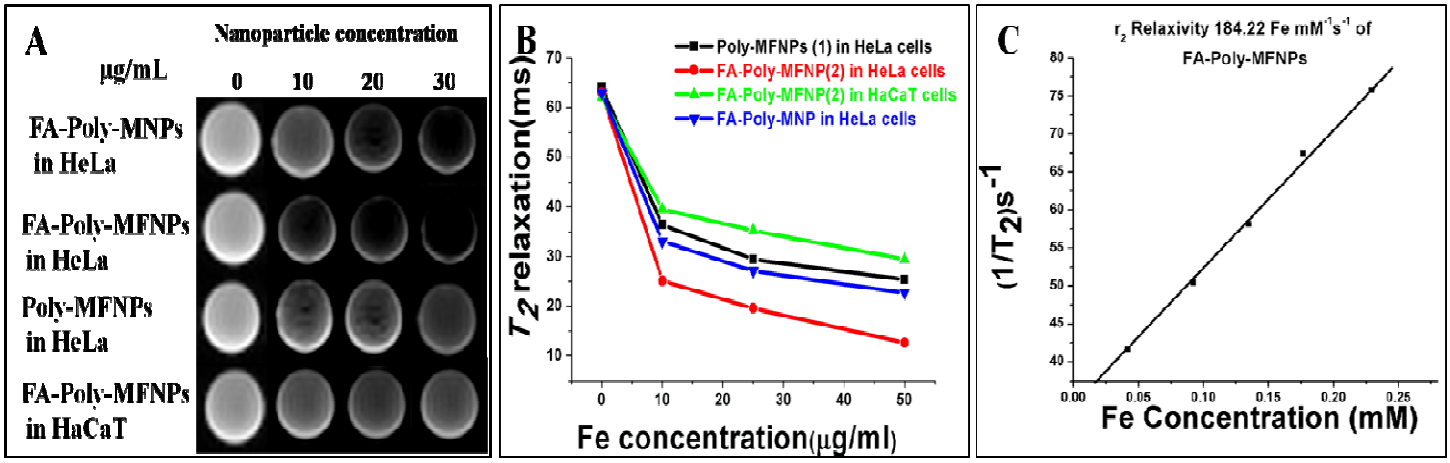

Fig. 6(A-C). A) T_2-weighted spin-echo MR phantom images of HeLa cells and HaCaT cells incubated with 0–30 µg/mL of various nanoparticle suspensions (FA-Poly-MNPs, Poly-MFNPs and FA-Poly-MFNPs) for 4h. FA-Poly-MNPs are the abbreviated form of FA targeted Polymer modified magnetite (Fe_3O_4) nanoparticles to compare the enhanced MR activity between mixed ferrite magnetic nanoparticles (MFNPs) and magnetite nanoparticles (MNPs). (B) T_2 relaxation analysis of HeLa and HaCaT cell suspensions of the FA-Poly-MFNPs, Poly-MFNPs and FA-Poly-MNPs. C) r2 Relaxivity analysis of FA-Poly-MFNPs with increasing Fe concentrations.

From the Fig. 7(A-F), it is evident that only FA-Poly-MFNPs (without DOX) has no apoptotic effect on HeLa cells in comparison whereas in free DOX, both the S phase population (24.44%) along with apoptotic Sub G_0/G_1 phase (6.0 %) population count has been increased. In case of DOX-FA-Poly-MFNPs, increasing concentrations of DOX-FA-Poly-MFNPs showed the maximum cell intensification at S phase, exhibiting cell cycle arrest in the same phase. In addition, the apoptotic Sub G_0/G_1 phase population also increases in a dose dependent manner in comparison to **2**.

Therefore, DOX-FA-Poly-MFNPs has inhibited the growth of HeLa cells by arresting cell cycle progression at S phase and followed to apoptosis or cell death. According to the previous reports, the DOX prevents cancer cell growth by inducing DNA breakage and arresting cell cycle at G_2/M phase [53] in HeLa cells. The deviation observed in our work, from previous reports may not be erroneous because free DOX also induced S phase arrest in our study. Again there are also reports that DOX molecules induced S phase arrest in other cancers cells like MCF-7 breast cancer cell line[54], so the possibility of S phase arrest by DOX treatment cannot be nullified.[55]

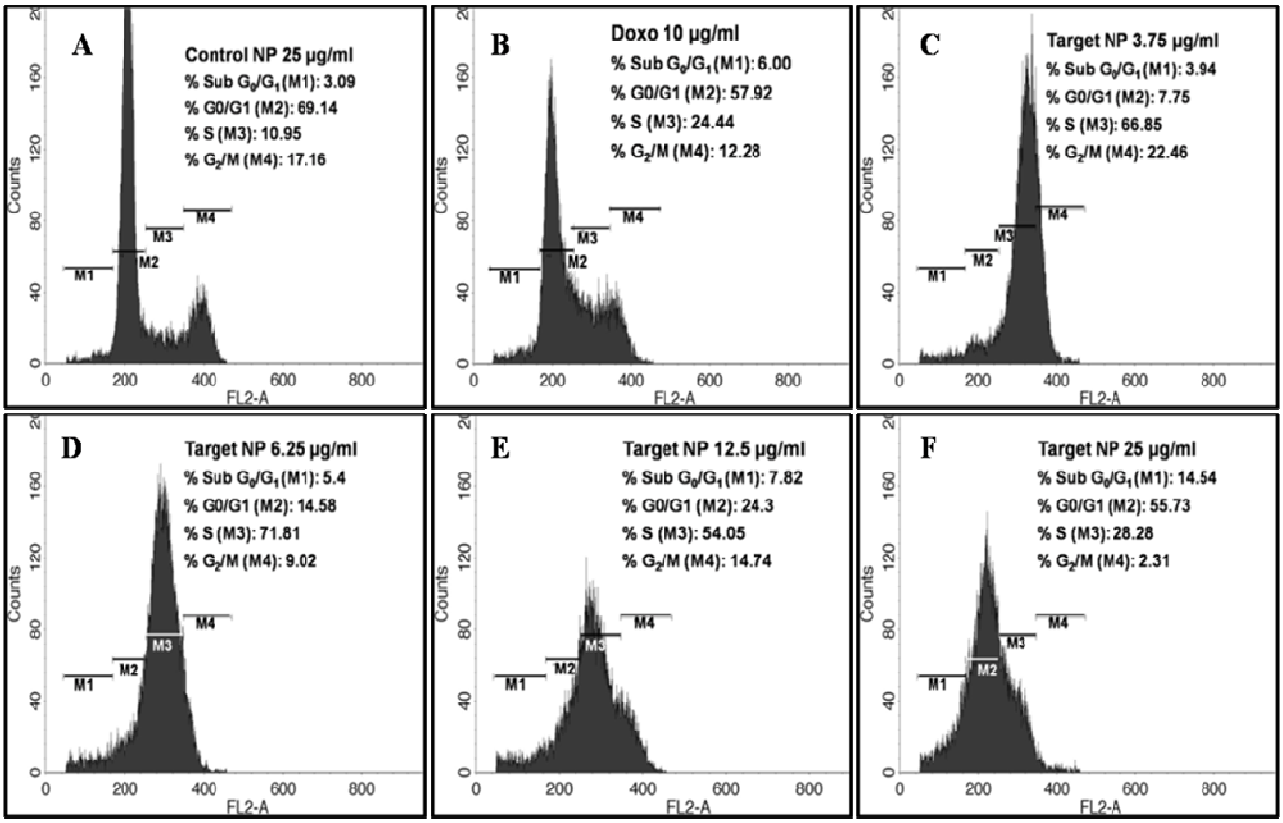

Fig. 7(A-F). Flow-cytometric analysis of cell cycle phase distribution. HeLa cells treated with (A) Control FA-Poly-MFNPs, (B) Bulk DOX 10 µg/ml, (C) Target DOX-FA-Poly-MFNPs (3.75 µg/ml) (D) 6.25 µg/ml E) 12.5 µg/ml and F) 25.0 µg/ml for 24 h. Diva software after the cells were labelled by PI preceding RNAase treatment and percentage of apoptosis was calculated.

With the aim of examining the nuclear morphology and identifying cell death in the path of apoptosis, HeLa cell nuclei were further stained with 4'-6-diamidino-2-phenylindole (DAPI), and the data was presented in Fig. 8(A-E). As predicted from the cytotoxicity experiments, the fluorescence images of HeLa cells, incubated with target nanoparticle without DOX (**2**) has shown that nuclear structures were well preserved without any visible abnormalities. [Fig. 8(A)] however, while treated with increasing concentration of DOX-Poly-FA-MFNPs, there was significant nuclei fragmentation which included condensed nucleus, membrane blebbing and formation of apoptotic bodies [(Fig. 8(B−E)]. It was also clearly visible that the quantity of apoptotic nuclei enhanced with an increasing concentration of DOX-Poly-FA-MFNPs. (apoptotic nuclei shown by arrow in the figure). There were previously acclaimed reports that doxorubicin interacts with DNA topoisomerase II (topo II) and can cause the accumulation of enzyme-DNA adducts that ultimately lead to double-strand breaks followed by programmed cell death or apoptosis [56-57]. In our case, the same pattern of nuclei fragmentation was observed after treatment of DOX-FA-Poly-MFNPs with HeLa cells.

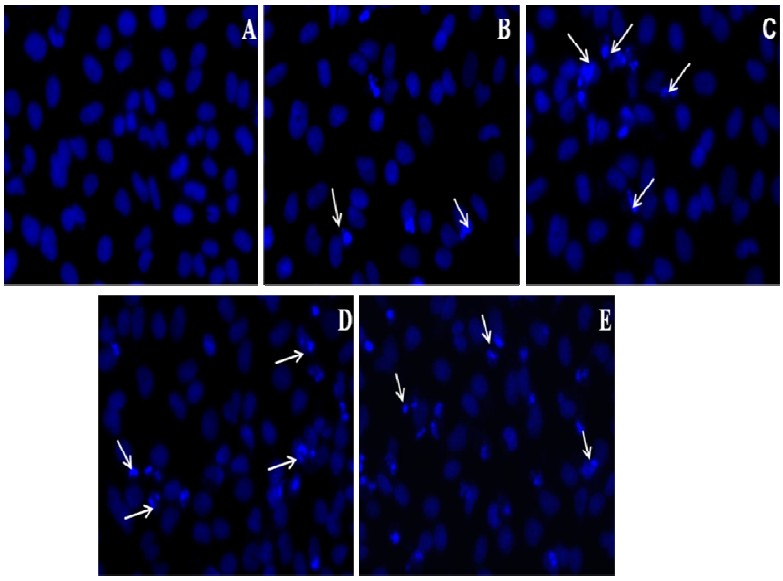

Fig.8. Apoptosis Study of DOX-FA-Poly-MFNPs by morphological changes in cell nuclei, determined by means of fluorescence microscopy after DAPI staining. HeLa cells were treated with (**A**) FA-Poly-MFNPs without DOX for 24 h and (**B**) 3.75 (**C**) 6.25 (**D**) 12.5 and **(E)** 25 μg/ml of DOX-FA-Poly-MFNPs for 24 h. Arrows indicate apoptotic nuclei.

3. CONCLUSION

In summary, stimuli responsive polymer integrated targeted nanomedicine was designed for combined cancer-targeted therapy and multimodal imaging by a facile preparation method. These nanoprobes were found to be potentially capable of dual pH and temperature responsive drug delivery, specifically targeted to cancer cells and also shown intracellular MR based diagnostic/tracking ability. These nanoprobes display a significant amount of drug entrapment inside the polymeric shell and initiate the release the drugs preferably at pH 5.5 and temperature 37 °C. The *in vitro* biological studies revealed that these nanoprobes are able to provide a single nanoconstruct, which is capable of simultaneously target, track and destroy folate-receptor over expressing cancer cells compared to the free drug. They

specifically accumulate inside the cancer cells through receptor mediated endocytosis, and the payloads can be released via the stimuli triggered nature of the fabricated nanoprobes. From the biological studies, it is envisioned the prepared nanohybrids comprised of cancer specific targeting, imaging, and therapeutic application in a single entity could be used as a theranostic platform for cancer treatment and may be of particular interest in near future.

4. EXPERIMENTAL SECTION

4.1. Materials

Pluronic F127 (F127, *Mw*: 12,600 KDa) were specially ordered from BASF, china. Succinic anhydride (SA), triethylamine (TEA), 4-dimethylaminopyridine (DMAP), branched Poly-(ethylenimine) (PEI, 25KDa), ferric chloride ($FeCl_3$), ferrous sulphate ($FeSO_4.7H_2O$), Trisodium Citrate, $MnCl_2.4H_2O$, EDBE, folic acid (FA), N-hydroxysuccinimide (NHS), 1-[3-(dimethylamino) propyl]-3-ethyl carbodiimide hydrochloride (EDC), trinitrobenzene sulfonic acid (TNBS), rhodamine isothiocyanate (RITC), Doxorubicin, 4'-6-Diamidino-2-phenylindole (DAPI), propidium iodide (PI), *RNase* and 3-(4,5-Dimethylthiazol-2-yl)-2,5-diphenyltetrazolium bromide (MTT) were purchased from Sigma-Aldrich Chemicals, USA. Commercially available dimethyl sulfoxide (DMSO) and N, N′-dimethyl formamide (DMF) were purified by vacuum distillation and dried 1,4-dioxane was distilled over sodium. Chloroform ($CHCl_3$) was procured from Merck, Germany. Fetal bovine serum and Minimum Essential Medium (MEM) were procured from Hyclone, USA and Himedia, India, respectively.

4.2. Methods

4.2.1. Synthesis of PEI crosslinked Pluronic F127 block copolymer (PEI–PF127)

For the synthesis of the PEI-PF127 block copolymer, the chemically inert PF127 was first modified by anhydride-acylation using SA.[58] For this, Anhydrous 2.5 g of Pluronic F127 was dissolved in 40 ml of 1,4 dioxane followed by the addition of 46 mg of SA, 50 mg of DMAP and 56 µl of TEA. The mixture was stirred under N_2 atmosphere for 24 h at room temperature. After solvent evaporation, white residue was obtained and these were then dissolved in chloroform to remove unreacted SA by filtration. The transparent solution was precipitated against excess cold diethyl ether in a dropwise manner. The precipitates were dried under vacuum and stored for later use. For the preparation of PEI-PF127 copolymer, briefly, a total of 100 mg of succinylated PF127, 100 mg of EDC, 100 mg of NHS were dissolved in 10 mL of Milli-Q water for 4 hrs under dark for carboxyl activation. Then, 10 mL aqueous solution of branched PEI (5.0 mg/mL) was added drop-wise to pre-activated PF127 solution at pH 5-5.5.[59] The mixture was further stirred for 24 h to allow the completion of cross-linking between the activated PF127 and PEI. The resulting mixture was dialyzed against distilled water at pH 6 for 3 days and lyophilized to obtain PEI-PF127. The obtained PEI-PF127 was confirmed by proton nuclear magnetic resonance (^{1}H NMR) analysis. (Given in ESI)

4.2.2 Preparation of Citrate stabilized MFNPs (CA-MFNPs) and PEI-PF127-MFNPs or Poly-MFNPs (**1**)

Magnetic mixed ferrite nanoparticles, here forth mentioned as CA-MFNPs in this paper, were prepared by a chemical coprecipitation approach according to our previously reported

procedure.[60] In brief, a mixture of $FeCl_3$ (0.324g), $FeSO_4 \cdot 7H_2O$ (0.140g) and $MnCl_2.4H_2O$ (0.098g) in a 4:1:1 ratio were dissolved in 40 ml deoxygenated Milli-Q water containing trisodium citrate (1mg/ml) in a three necked flask equipped with argon flow and a mechanical stirrer. To this, ammonium hydroxide (5 ml) was added dropwisely and the mixture was stirred for 4 h at 70 °C. After completion of the reaction, black CA-MFNPs were recovered and washed thoroughly with Milli-Q water followed by drying.

The previously synthesized PEI-PF127 was covalently conjugated to the CA-MFNPs via the well established EDC/NHS method. In brief, 0.1g of CA-MFNPs was dispersed ultrasonically in 20 ml Milli-Q water for 30 mins and was activated with 0.1g of NHS and 0.1g of EDC under dark for 4h. To this solution, 20 ml of PEI-PF127 (5 mg/ml) was added drop wise under ultrasonication at pH around 5-6 followed by stirring for 24 hrs. Subsequently, these aminated Poly-MFNPs (**1)** were finally recovered through magnetic separation, washed with Milli-Q water, and followed by drying.

4.2.3. Preparation of Folic acid (FA) Tethered Polymer modified MFNPs (FA-Poly-MFNPs)

Folic acid tethering to Poly-MFNPs was carried out via EDC/NHS chemistry according to a reported procedure with a little modification.[44-45] In a typical synthesis, 100mg of FA (0.22 mM) was dissolved in 10 mL of DMSO-Milli Q water mixture (1:1 v/v) and pH was maintained at 8-10 using dilute NaOH. To the above FA solution, activation was carried out using EDC (100 mg, 0.48 mM) and NHS (56 mg, 0.48 mM) for 4 h under dark condition. Subsequently, 100 mg aqueous dispersion of Poly-MFNPs (**1**) was added to it and the resulting mixture was stirred overnight in dark at RT. At last, the FA modified Poly-MFNPs (FA-Poly-MFNPs) were magnetically concentrated, washed several times with Milli Q water as well as DMSO and at last, recovered.

4.2.4. Doxorubicin loading Studies

For DOX loading, 10 mg of FA-Poly-MFNPs (**2**) was added to a 10 ml of 0.5mg/mL DOX solution, and the mixture was kept in a shaker for 48 h under dark conditions. Finally, the DOX loaded FA-Poly-MFNPs (**3**) were recovered using magnetic decantation followed by repetitive centrifugation and washed thrice with distilled water to remove unbound DOX molecules. For the synthesis of DOX-Poly-MFNPs, similar amount of DOX solution was incubated with the same concentration of Poly-MFNPs (10mg) and the same procedure was repeated as followed for DOX-FA-Poly-MFNPs. In both the cases, the supernatant was collected to determine the drug loading content and drug encapsulation efficiency (EE) from UV−Vis absorbance at 480 nm. The amount of DOX entrapped was determined from a calibration curve previously made using DOX solutions of different concentrations. The drug loading content and entrapment efficiency were determined by the following equations:

$$\text{Drug loading contents (\%):} \quad \frac{\text{Weight of drug in nanoparticles} \times 100}{\text{Weight of prepared nanoparticles}}$$

$$\text{Drug entrapment efficiency (\%):} \quad \frac{\text{Weight of drug in NPs} \times 100}{\text{Weight of drug injected}}$$

4.2.5. Preparation of RITC labelled FA-Poly-MFNPs (Fluorescent conjugates of **1** and **2**)

For the fluorescent labelling, a portion of the FA-Poly-MFNPs (**2**) mentioned above, were covalently linked with rhodamine isothiocyanate (RITC), a highly fluorescent molecule, using the residual amine groups of FA-Poly-MFNPs via covalent conjugation approach. For this, 1mg of rhodamine isothiocyanate (RITC) dissolved in 1ml of DMSO-H_2O mixture was added drowse to an aqueous suspension of FA-Poly-MFNPs (10mg) at pH 8. The resulting suspension was sonicated for an hour and stirred for 12 hr in the dark. Particles were

recovered by magnetic decantation followed by centrifugation and washed thoroughly with deionized water to remove any unreacted or physically bound RITC molecules. These particles were labelled as RITC-FA-Poly-MFNPs (**3**). Similar labelling was also done with MFNPs without folic acid modification (RITC-Poly-MFNPs) in the as described manner and used as a control for an imaging study.

4.2.6. Release of Doxorubicin from nanoparticles

The cumulative drug release profile of DOX from the DOX-FA-Poly-MFNPs (**4**) was carried out at four different conditions to evaluate the stimuli-response behaviour of the nanohybrids towards pH and temperature. The release of DOX from the DOX-loaded MFNPs was carried out under the physiological pH (in pH~7.4) at two different temperatures 25°C and at 37°C and also lysosomal pH condition (pH~5.5) using the same temperatures. For each experiment, 10 mg of DOX-FA-Poly-MFNPs was dispersed in 5 mL of phosphate buffer (pH ~7.4) or in phosphate-citrate buffer (pH ~5.5) and incubated in the above-mentioned temperature. Then they were dialyzed against distilled water in different pH and temperatures in a shaking bath kept in the dark using membrane of molecular weight cut-off of 12 kDa. The released DOX from solution was assayed spectrophotometrically by measuring the absorbance of the solution at 480 nm collected at specific time intervals. The samples taken for measurement were returned to the receiver solution after measurement. The percentage of released drug was calculated from a standard curve of free drug solution. The data were expressed as the mean value of three independent experiments with the standard deviation.

4.2.7. Cell lines and Cytotoxicity Studies

The biocompatibility of the FA-Poly-MFNPs (**2**) and DOX-FA-Poly-MFNPs (**4**) was evaluated by standard MTT [3-(4,5-dimethylthiazol-2-yl)-2,5-diphenyltetrazolium bromide] assay. Two types of cells cultivated for *in vitro* experiments were HeLa (human cervix adenocarcinoma) and HaCaT (immortalized human keratinocyte), which were acquired from the National Centre for Cell sciences (NCCS), Pune, India. It is mentioned that the as received HeLa cells was used as HeLa cells expressing High Folate receptor (HeLa-HFAR) cells. HeLa cells expressing Low Folate receptor (HeLa-LFAR) cells were prepared from incubation of free folic acid in medium. These cells were cultured in Minimum Essential Medium (MEM) and Dulbecco's Modified Eagle's medium (DMEM) medium supplemented with 10% fetal calf serum, penicillin (100 units/mL), streptomycin (100mg/mL), and 4mM L-glutamine at 37ºC in tissue culture flasks in a 5% CO_2 and 95% air humidified atmosphere. For the cytotoxicity experiment, trypsinized cells were adjusted to a concentration of 1×10^5 cells/mL and plated in a 96 well flat bottom culture plates (180µl/well). For toxicity studies, both the cells were incubated with DOX-FA-Poly-MFNPs, DOX-Poly-MFNPs and FA-Poly-MFNPs for 24 h at 37 ºC in a humidified 5% CO_2 incubator. Then MTT was added and plates were incubated for 4 h under the dark. The resulting formazon crystals were solubilised by dissolving in an MTT solubilization buffer. Then, the absorbance was measured at 570 nm by using a (Biorad) microplate reader and the values were compared with respect to control cells. Mean and standard deviation for the triplicate wells were reported.

With the aim to confirm the targeting efficacy of the DOX-FA-Poly-MFNPs,[52] approximately 1×10^5 cells per well were seeded in 96-well plates the day before the

experiments to bring the cells to confluence. Then, the DOX-FA-Poly-MFNPs or DOX-Poly-MFNPs with same concentration (25μg/ml) were separately added to both HeLa-HFAR and HeLa-LFAR cells, the medium in wells containing the complexes was totally taken out and replenished with the same volume of fresh medium after 2 h incubation. The cells were then incubated for 48 h at 37 °C. After that, an MTT assay was used to quantify the viability of cells. The assays were carried out according to the manufacturer's instructions. Mean and standard deviation for the triplicate wells were reported.

4.2.8. Intracellular Uptake Studies

The folate mediated internalization of RITC-Poly-MFNPs and RITC-FA-Poly-MFNPs by a folate receptor overexpressed HeLa cancer cell i.e. HeLa-HFAR (positive control) and a normal human keratinocyte HaCaT cells were demonstrated by fluorescence microscopy. For time dependent uptake studies, 10μg/mL MFNPs of each types were incubated with folate receptor positive (FAR) HeLa cells (HeLa-HFAR cells) in variant times (0, 30 min, 1 h, 2 h and 4 h). After incubation, HeLa-HFAR cells cells were fixed with 4% paraformaldehyde for 15 min, permeabilized with 0.1% Triton X-100, and stained with DAPI (1 mg/ml) for 5 min at 37^{o}C. The cells were then washed with PBS and examined by time dependent fluorescence microscopy (Olympus IX 70). Likewise, for the evaluation of the FAR receptor specificity of HeLa cells, intracellular uptake of RITC-FA-Poly-MFNPs was cross checked using both the HeLa-HFAR and receptor negative FA (-) HaCaT cells for 4h and studied via Fluorescence imaging. (Detailed Data and description was given as Figure S9 in ESI). The FAR targeting efficiency of FA-RITC-Poly-MFNPs was also validated using HeLa-HFAR and HeLa-LFAR (preincubated with free folic acid). (Data was shown in ESI as Figure S10).

4.2.9. Cell Cycle Analysis

For the evaluation of the therapeutic efficacy of the DOX-FA-Poly-MFNPs (**4**), concentration dependent cell-cycle analysis was performed in HeLa-HFAR cells. Cells (1×10^5) were treated with different concentration (3.25, 6.25, 12.5 and 25 μg/ml) of **4** for 24 h at 37 °C. The cells were harvested and fixed in 70% ethanol stored at –20 °C. Then, the cells were washed with ice-cold PBS (10 mM, pH 7.4) and resuspended in 200 μL of PBS followed by incubation with 20 μl *DNAase* free *RNase* (10 mg/mL) and 20 μl of DNA intercalating dye PI (1 mg/mL) at 37 °C for 1 h in dark. Apoptotic cells were determined by their hypochromic sub-diploid staining profiles. The distribution of cells in the different cell-cycle phases was analyzed from the DNA histogram using Becton-Dickinson FACS Calibur Flow Cytometer and Cell Quest software.

4.2.10. DAPI Staining for Nuclear Morphology Study

For visualization of HeLa cells, the cell nucleus was stained with DAPI. The DAPI staining was performed to corroborate the apoptotic effect of **4** on HeLa-HFAR cells. For this, HeLa cells were treated with PBS (control set) and (3.25, 6.25, 12.5 and 25 μg/mL) of DOX-FA-Poly-MFNPs for 24 h at 37 °C. After this, cells were fixed with 3.7% formaldehyde for 15 min, permeabilized with 0.1% Triton X-100 and stained with 1μg/mL DAPI for 5 min at 37 °C. The cells were then washed with PBS and examined under fluorescence microscopy (Olympus IX 70).

4.2.11. In vitro cellular MR imaging

Samples for MR phantom imaging were prepared by suspending 10^6 cells in low-melting 1% agarose gel (50 mL).[45] MRI was performed with a 1.5 T clinical MRI scanner (GE Medical

systems, Milwaukee) using a prefabricated sample holder. A spin-echo multi-section pulse sequence was selected from the GE Medical systems to acquire MR phantom images. A repetition time (TR) of 2100 ms and variable echo times (TE) of 42–110 ms were used. The spatial resolution parameters were set as follows: an acquisition matrix of 256×256, field of view of 240×240 mm^2, section thickness of 8 mm, and two averages. The MRI signal intensity (SI) was measured using the in-built software. T_2 values were obtained by plotting the SI of each sample over a range of TE values. T_2 relaxation times were then calculated by fitting a first-order exponential decay curve to the plot. The fitting equation can be expressed as $SI=Ae^{-TE/T_2} + B$....Equation 1, where SI is the signal intensity, TE is the echo time, A is the amplitude and B is the offset. The relaxivity, the R_2 value, was also calculated plotting the inverse of T_2 with respect to Fe concentration, according to the following equation, $1/T_2 = 1/T_2\ (_0) + r_2\ [Fe]$.....Equation 2, where $1/T_2$ is the observed transverse relaxation rate in the presence of magnetite nanoparticles, $1/T_2\ (_0)$ is the relaxation rate of pure water, [Fe] is the concentration of magnetite nanoparticles and r_2 denotes transverse relaxivities.

5. CHARACTERIZATIONS

The surface chemistry and chemical structures of products were analyzed from FTIR and ^1H NMR (Bruker, 400 MHz) spectra. The FTIR of the biofunctionalized nanoparticles were recorded in KBr in the range 400–4000 cm^{-1} with a model Nexus-870, Thermo Nicolet Corporation, Wisconsin, USA. The phase analysis of the synthesized mixed ferrite nanopowder was performed on an X'pert Pro Phillips X-ray diffractometer. The sample for XRD was prepared by the deposition of well dispersed nanoparticles on a glass slide and, after drying, the analysis was performed by using Ni-filtered Cu-Kα radiation (I = 1.54 A^0). The size and morphology of the nanoparticles were observed by high-resolution transmission

electron microscopy (HRTEM) (JEOL 3010, Japan) operated at 200 KV. The nanoparticles were thoroughly dispersed in water by ultra-sonication (1 mg/50 ml Milli Q water) and a drop of the solution was placed on carbon coated copper grid. The average particle size from TEM micrographs was analyzed using image J software. Surface composition of nanoparticles was obtained from X-ray photoelectron spectroscopic (XPS) analysis using an Al Ka excitation source in an ESCA-2000 Multilab apparatus (VG microtech). The sample used in XPS prepared in the similar procedure as used in TEM. TNBS assay was used to determine the percentage of primary amines in the NPs solution. The $–NH_2$ group concentration was calculated by a graph originated by taking glycine (0-2 mmol) as standard[61]. To determine the extent of folate conjugation, UV-Vis spectra were recorded by spectrophotometric analysis of absorbance at 286 nm and 360 nm and also cross-checked by determination of residual amine concentration via TNBS assay. The Dynamic Light Scattering (DLS) measurements at different temperatures and pHs were done using Brookhaven 90 Plus particle size analyzer. The surface charge of the nanoparticles was investigated through zeta potential measurements (Zetasizer 4, Malvern Instruments, UK). Thermal analysis was done with a thermal analyzer (Pyris Diamond TG/DTA) with a heating rate 8 °C min^{-1} with in temperature range 50 °C to 1000 °C. Magnetic measurements of nanoparticles were performed using a SQUID-VSM instrument (Ever cool SQUID VSM DC Magnetometer).

SUPPORTING INFORMATION.

Detailed tables of DLS after modification with PEI-PF127 and FA, and amine quantification results, Change of zeta potential with pH, dual pH and Temperature responsive transition of HDs of FA-Poly-MFNPs and Poly-MFNPs at fixed temperature as well as pH, FT-IR, UV-Vis Spectra, TGA, XPS, VSM analysis were given. Cell viability assays of Poly-MFNPs and

FA-Poly-MFNPs in cancer HeLa and normal HaCaT cell lines and intracellular uptake of RITC labeled FA-Poly-MFNPs in presence and in absence of free FA. ^{1}HNMR of the block copolymer PEI-PF127 is given as Figure S12 which was used for the surface modification with CA-MFNPs,

ACKNOWLEDGEMENTS

The authors gratefully acknowledge Dr K. R. Patil, Centre of Material Characterization, National Chemical Laboratory (NCL), Pune, for assistance with the XPS studies. Authors are thankful to Eco MRI, Kolkata for *in vitro* MR imaging studies. Authors are grateful to the both CSIR New Delhi and DST Nano Mission for providing research fellowship and financial support for this work.

Received: ((will be filled in by the editorial staff))
Revised: ((will be filled in by the editorial staff))
Published online: ((will be filled in by the editorial staff))

NOTES AND REFERENCES

1 L. Y. Zhang, R. Guo, M. Yang, X. Q. Jiang and B. R. Liu, *Adv. Mater,* 2007, **19**, 2988.

2 K. S. Soppimath, D. C.W. Tan and Y.Y. Yang, *Adv. Mater,* 2005, **17**, 318.

3 V. Bagalkot, L. F. Zhang, E. Levy-Nissenbaum, S. Jon, P. W. Kantoff, R. Langer and O. C. Farokhzad, *Nano Lett,* 2007, **7**, 3065.

4 H. S. Choi, K. M. Huh, T. Ooya and N. Yui, *J. Am. Chem. Soc,* 2003, **125**, 6350.

5 O. J. Cayre, N. Chagneux and S. Biggs, *Soft Matter,* 2011, **7**, 2211.

6 M.C. Daniel and D. Astruc, *Chem. Rev,* 2004, **104**, 293.

7 X. Wu, Z. Wang, D. Zhu, S. Zong, L. Yang, Y. Zhong and Y.Cui, *ACS Appl Mater Interfaces*, 2013, **5**, 10895.

8 X. Liu, D. Yu, C. Jin, X. Song, J. Cheng, X. Zhao, X. Qi and G. Zhang, *New J. Chem.*, 2014**, 38,** 4830**.**

9 K. Yan, P. Li, H. Zhu, Y. Zhou, J. Ding, J. Shen, Z. Li, Z. Xu and P. K. Chu, *RSC Adv,* 2013**, 3,** 10598**.**

10 H. Meng, M. Xue, T. Xia, Y. L. Zhao, F. Tamanoi, J. F. Stoddart, J. I. Zink, and A. E. Nel, *J. Am. Chem. Soc,* 2010, **132**, 12690.

11 H. Ai, C. Flask, B.; Weinberg, X. T. Shuai, M. D. Pagel, D. Farrell, J. Duerk and J. Gao, *Adv. Mater*, 2005, **17**, 1949.

12 J.H.; Park, G. v. Maltzahn, L. Zhang, M. P. Schwartz, E. Ruoslahti, S. N. Bhatia, M. J. Sailor, *Adv. Mater*, 2008, **20**, 1630.

13 P. Guardia, R. D. Corato, L. Lartigue, C. Wilhelm, A. Espinosa, M. G. Hernandez, F. Gazeau, L. Manna and T. Pellegrino, *ACS Nano*, 2012**, 6***,* 3080.

14 X. Yang, S. Pilla, J. J. Grailer, D. A. Steeber, S. Gong, Y. Chen and G. Chen, *J. Mater. Chem,* 2009*,* **19***,* 5812.

15 J. M. Yang, C.H. Lee, H.J. Ko, J. S. Suh, H. G. Yoon, K. Lee, Y.M. Huh, and S. Haam, *Angew. Chem. Int. Ed,* 2007, **46**, 8836.

16 M. K. Yu, Y. Y. Jeong, J. Park, S. Park, J. W. Kim, J. J. Min, K. Kim and S. Jon, *Angew. Chem., Int. Ed.* 2008, **47**, 5362.

17 W. H. Chiang, V. T. Ho, W. C. Huang, Y. F. Huang, C. S. Chern and H. C. Chiu, *Langmuir*, 2012, **28**, 15056.

18 D. Y. Chen, X. W. Xia, H. W. Gu, Q. F. Xu, J. F. Ge, Y. G. Li, N. J. Li and J. M. Lu, *J. Mater. Chem*, 2011, **21**, 12682.

19 L. E. Gerweck and K. Seetharaman, *Cancer Res,* 1996, **56**, 1

20 X. Hu, X. Hao, Y. Wu, J. Zhang, X. Zhang, P. C. Wang, G. Zou and X. J. Liang, *J. Mater. Chem. B,* 2013, **1,** 1109.

21 C. S. Brazel, *J. Pharm. Sci,* 2009, **26**, 644.

22 D. Yoo, J. H. Lee, T. H. Shin and J. Cheon, *Acc. Chem. Res,* 2011, **44**, 863.

23 A. Popat, J. Liu, G. Q. M. Lu and S. Z. Qiao, *J. Mater. Chem,* 2012, **22**, 11173.

24 X. Mei, D. Y. Chen, N. J. Li, Q. F. Xu, J. F. Ge, H. Li, B. X. Yang, Y. J. Xu and J. M. Lu, *Soft Matter,* 2012, **8**, 5309.

25 H. C. Dong, V. Mantha and K. Matyjaszewski, *Chem. Mater,* 2009, **21**, 3965.

26 T. Isojima, M. Lattuada, J. B. Vander Sande and T. A. Hatton, *ACS Nano*, 2008, **2**, 1799.

27 S. Chen, Y. Li, C. Guo, J. Wang, J. H. Ma, X. F. Liang, L. R. Yang and H. Z. Liu. *Langmuir* 2007, **23**, 12669.

28 J. J. Lai, J. M. Hoffman, M. Ebara, A. S. Hoffman, C. Estournes, A. Wattiaux, and P. S. Stayton, *Langmuir* 2007, **23**, 7385–7391.

29 S. Bhattacharya, F. Eckert, V. Boyko and A. Pich, *Small* 2007, **3***,* 650.

30 F. Zhang and C. C. Wang, *Langmuir* 2009, **25**, 8255.

31 B. Sahoo, S. Devi, R. K. Banerjee, T.K. Maiti, P. Pramanik and D. Dhara, *ACS Appl Mater Interfaces*. 2013, **5**, 3884.

32 G. Wanka, H. Hoffmann and W. Ulbricht, *Macromolecules,* 1994, **27**, 4145.

33 S. Patra, E. Roy, P. Karfa, S. Kumar, R. Madhuri and PK Sharma, *ACS Appl Mater Interfaces,* 2015, **7***,* 9235.

34 A. V. Kabanov, E. V. Batrakova and V. Y. Alakhov, *J. Controlled Release,* 2002, **82**, 189.

35 S. H. Choi, S. H. Lee and T. G. Park, *Biomacromolecules*, 2006, **7**, 1864.

36 S. H. Lee, S. H. Choi, S. H. Kim and T. G. Park, *J. Controlled Release*, 2008, **125**, 25.

37 W. Zhang, K. Gilstrap, L. Wu, K. C. R. Bahadur, M.A. Moss, Q. Wang, X. Lu and X. He, *ACS Nano,* 2010, **4**, 6747.

38 L. Yang, C. Guo, _ L. Jia, X. Liang, C. Liu and H. Liu, *J. Colloid Interface Sci*, 2010, **350**, 22.

39 M. Thomas and A. M. Klibanov, *Proc. Natl. Acad. Sci. U.S.A.* 2002, **99**, 14640.

40 J. W. Park, K. H. Bae, C. Kim and T. G. Park, *Biomacromolecules*, 2011, **12**, 457.

41 U. I. Tromsdorf, N. C. Bigall, M. G. Kaul, O. T. Bruns, M. S. Nikolic, B. Mollwitz, R. A. Sperling, R. Reimer, H. Hohenberg, W. J. Parak, S. Fo1rster, U. Beisiegel, G. Adam and H. Weller, *Nano Lett***, 2007**, **7**, 2422.

42 S. D. Li and L. Huang, *Mol. Pharmaceutics,* 2008, **5**, 496.

43 B. Chertok, A. E. David and V. C. Yang, *Biomaterials,* 2010, **31**, 6317.

44 P. Singh, U. Gupta, A. Asthana and N. K. Jain, *Bioconjugate Chem*, 2008, **19**, 2239.

45 D. Bhattacharya, M. Das, D. Mishra, I. Banerjee, S. K. Sahu, T. K. Maiti, and P. Pramanik. *Nanoscale,* 2011**, 3,** 1653.

46 Y. L. Su, J. Wang and H. Z. Liu, *J. Phys. Chem. B*, 2002*,* **106***,* 11823.

47 K. Nawara, J. Romiszewski, K. Kijewska, J. Szczytko, A. Twardowski, M. Mazur and P. Krysinski, *J. Phys. Chem.* C, 2012, **116***,* 5598.

48 J. Zhang, S. Rana, R. S. Srivastava and R. D. K. Misra, *Acta Biomater.* 2008, **4**, 40.

49 X. Yang, J. J. Grailer, I. J. Rowland, A. Javadi, S. A. Hurley, D. A. Steeber and S. Gong, *Biomaterials,* 2010**, 31**, 9065.

50 X. Yang, J. J. Grailer, I. J. Rowland, A. Javadi, S. A. Hurley, V. Z. Matson, D. A. Steeber and S. Gong, *ACS Nano*, 2010, **4**, 6805.

51 J. H. Lee, Y.M. Huh, Y.W. Jun, J.W. Seo, J.T. Jang, H.T. Song, S. E. Kim, J. Cho, H. G. Yoon, J. S. Suh and J. Cheon. *Nat. Med,* 2007, **13**, 95.

52 S. Wen, H. Liu, H. Cai, M. Shen and X. Shi. *Adv. Healthcare Mater.* 2013, **2**, 1267.

53 Y. H. Ling, A. K. el-Naggar, W. Priebe and R. Perez-Soler, *Mol. Pharmacology*, 1996, **49,** 832**.**

54 O. Bar-On, M. Shapira and D. D. Hershko, *Anticancer drugs*, 2007, **18**, 1113.

55 T. J. Westmoreland, S. M. Wickramasekara, A. Y. Guo, A. L. Selim, T. S. Winsor, A. L. Greenleaf, K. L. Blackwell, J. R. Marks and C. B. Bennett, *PloS One*, 2009, **4**, e5830.

56 A. Bodley, L. F. Liu and M. Israel, *Cancer Res.* 1989, **49**, 5969.

57 I. G. Cowell, A. L. Okorokov, S. A. Cutts, K. Padget, M. Bell, J. Milner, and C. A. Austin, *Exp. Cell Res,* 2000, **255**, 86.

58 Y. H. Bae, K. M. Huh, Y. Kim and K.H. Park, *J. Controlled Release***,** 2000, **64**, 3.

59 K. M. Park, J. W. Bae, Y. K. Joung, J. W. Shin and K. D. Park, *Colloid Surf. B*, 2008, **63**, 1.

60 D. Bhattacharya, A. Baksi, I. Banerjee, R. Ananthakrishnan, T. K. Maiti, and P. Pramanik. *Talanta*, 2011, **86**, 337.

61 F. E. Levy, M. C. Andry and M. C. Levy, *Int. J. Pharm.* 1993, **96**, 85.

TOC: Stimuli triggered release of DOX from dual responsive theranostic nanocarriers mimicking lysosomal condition i.e. physiological temperature (37°C) and acidic pH (5.5).